

Effect of surface treatments on electrical properties of β -Ga₂O₃

Jiancheng Yang, Zachary Sparks, Fan Ren, Stephen J. Pearton, and Marko Tadjer

Citation: *Journal of Vacuum Science & Technology B* **36**, 061201 (2018); doi: 10.1116/1.5052229

View online: <https://doi.org/10.1116/1.5052229>

View Table of Contents: <http://avs.scitation.org/toc/jvb/36/6>

Published by the [American Vacuum Society](#)

Articles you may be interested in

[A review of Ga₂O₃ materials, processing, and devices](#)

Applied Physics Reviews **5**, 011301 (2018); 10.1063/1.5006941

[Guest Editorial: The dawn of gallium oxide microelectronics](#)

Applied Physics Letters **112**, 060401 (2018); 10.1063/1.5017845

[Structural and electronic properties of Ga₂O₃-Al₂O₃ alloys](#)

Applied Physics Letters **112**, 242101 (2018); 10.1063/1.5036991

[Breakdown mechanism in 1 kA/cm² and 960 V E-mode \$\beta\$ -Ga₂O₃ vertical transistors](#)

Applied Physics Letters **113**, 122103 (2018); 10.1063/1.5038105

[Acceptor doping of \$\beta\$ -Ga₂O₃ by Mg and N ion implantations](#)

Applied Physics Letters **113**, 102103 (2018); 10.1063/1.5050040

[On the feasibility of p-type Ga₂O₃](#)

Applied Physics Letters **112**, 032108 (2018); 10.1063/1.5009423



Contact Hiden Analytical for further details:
W www.HidenAnalytical.com
E info@hiden.co.uk

CLICK TO VIEW our product catalogue

Instruments for Advanced Science




Gas Analysis

- dynamic measurement of reaction gas streams
- catalysis and thermal analysis
- molecular beam studies
- dissolved species probes
- fermentation, environmental and ecological studies



Surface Science

- UHV-TPD
- SIMS
- end point detection in ion beam etch
- elemental imaging - surface mapping



Plasma Diagnostics

- plasma source characterization
- etch and deposition process reaction kinetic studies
- analysis of neutral and radical species



Vacuum Analysis

- partial pressure measurement and control of process gases
- reactive sputter process control
- vacuum diagnostics
- vacuum coating process monitoring

Effect of surface treatments on electrical properties of β -Ga₂O₃

Jiancheng Yang,¹ Zachary Sparks,¹ Fan Ren,¹ Stephen J. Pearton,^{2,a)} and Marko Tadjer³

¹Department of Chemical Engineering, University of Florida, Gainesville, Florida 32611

²Department of Materials Science and Engineering, University of Florida, Gainesville, Florida 32611

³Naval Research Laboratory, Washington, DC 20375

(Received 15 August 2018; accepted 17 September 2018; published 28 September 2018)

The effect of various combinations of gaseous (ultraviolet/O₃), liquid (HCl, buffered oxide etch, and H₂O₂), or plasma (CF₄ and O₂) treatments of the surface of β -Ga₂O₃ was quantified by current–voltage and capacitance–voltage measurements of rectifier structures. Plasma exposure (13.56 MHz, 24 kW/cm²) always led to significant degradation of the surface, as evidenced by large increases in rectifier reverse current and ideality factor (from 1.01 in control samples to ~3.8 in plasma exposed samples, indicating additional defect-related carrier transport mechanisms) and lowering of the Schottky barrier height (from 1.21 eV in control samples to 0.75–0.86 eV in plasma exposed samples) and diode rectification ratio, with degraded reverse recovery characteristics. This was true of both CF₄ and O₂, even though it is known that fluorine incorporation in the near-surface leads to donor compensation and an increase in barrier height. Damage from the plasma exposure was not fully recovered by annealing at 500 °C. The O₃ and liquid chemical cleans did lead to reduced reverse current in rectifiers, with no measurable decrease in barrier height, increase in ideality factor, or degradation of reverse recovery characteristics. Surfaces treated in this manner did not significantly change for anneals up to 500 °C; however, the Ni/Au contacts already show degradation after annealing at 350 °C. Published by the AVS. <https://doi.org/10.1116/1.5052229>

I. INTRODUCTION

β -Ga₂O₃ has properties that make it attractive for power switching electronics.^{1–12} In power conversion systems, the key components for transferring electricity between its AC and DC forms and changing its voltage and frequency are the power transistor and the diode.^{13–18} High voltage power conditioning systems to convert between DC and 60 Hz AC are needed throughout a modern energy grid/distribution system, e.g., DC–AC and AC–AC conversion, and conditioning is necessary to connect the electric grid to wind-turbine farms, fuel-cell storage, thermal energy storage, and hydroelectric dams, as well as plug-in electric vehicles.^{13–15} Currently, commercial SiC metal oxide semiconductor field effect transistor switches and Schottky diodes are available up to 12 kV, 60 A at 20 kHz, and operational to 50 kHz at lower currents. Even higher voltages of 15 kV (at 5 kHz) are obtainable with SiC insulated gate bipolar transistor switches and SiC PiN diodes.^{13–15} There are also numerous military applications, e.g., SiC power devices are used in U.S. Navy DDG 1000 Zumwalt Class destroyers to supply 78 MW at 4160 V.^{15,16} GaN is also making inroads in power conversion systems (1200 V parts first appeared in 2012) due to the high mobility that allows operation beyond 2 MHz, enables large step down ratios in buck converters, and decreases passive component sizes.^{17,18} Ga₂O₃ has an even larger bandgap than SiC or GaN and shows promising high power device performance.

In addition to power switching, Ga₂O₃ is well-suited to ultraviolet (UV) photodetectors, with applications in flame sensors, missile detection and guidance radiation detectors, secure satellite communications, and analysis in chemical,

environmental, and biological fields.^{2,4,6,9} Deep-UV photodetectors with solar blindness (cutoff wavelength of 280 nm, i.e., 4.43 eV) are preferred for applications in fire detection and military surveillance. Si- and GaAs-based deep-UV photodetectors are not truly solar-blind, as additional visible-light blocking filters are required due to their bandgaps. Commercial solar-blind optical devices are bulky, fragile, and only operational under large bias conditions.

A key aspect of making Ga₂O₃ devices for power switching or UV detection is the ability to process the material without degrading its electrical properties.^{4,10,11} β -Ga₂O₃ crystals have monoclinic symmetry with the space group being *C2/m*.² There are two inequivalent gallium sites and three inequivalent oxygen sites.² Ga(I) ions have four oxygen neighbors, and the Ga(II) ions have six oxygen neighbors. O(I) and O(II) ions have three gallium neighbors, and the O(III) ions have four gallium neighbors. The difference in volatility between Ga and O and the number of potential native defects possible mean that it is important to establish the stability of the materials during surface cleaning and etching steps. To date, there is little published work on this area. Yao *et al.*¹⁹ investigated wet chemical surface cleaning treatments prior to Schottky metallization and concluded that rinsing in an organic solvent, cleaning with HCl and H₂O₂, and rinsing with deionized water produced the most reproducible contacts. Others have reported a sequence of buffered oxide etch (BOE), HF (46%) and H₂SO₄/H₂O₂ or H₂SO₄/H₂O₂, followed by BOE.^{20–23} Based on experience, it is likely that most air-exposed Ga₂O₃ surfaces will have a contamination layer consisting of GaO_x and adsorbed carbons. It has long been established that UV/O₃ oxidation is effective for removing carbon from semiconductor surfaces,

^{a)}Electronic mail: spear@mse.ufl.edu

while the aggressive H₂O₂/H₂SO₄ (Piranha solution) can also remove gross carbon contamination from these surfaces. Additional work on establishing the effect of different liquid, gas, and plasma treatments is desirable.

In this paper, we use electrical measurements (current–voltage, capacitance–voltage, and reverse recovery) on Schottky rectifiers treated with different chemicals prior to metallization to establish surface stability of β -Ga₂O₃. The contamination layer on Ga₂O₃ epilayers will behave as a barrier to carrier transport through the Ga₂O₃/metal interface.^{24–29} For example, in Si, GaAs, and InP metal oxide semiconductor diodes, thin oxide layers provide energy barriers for carrier injection. In our work, plasma treatments are shown to severely degrade the Schottky characteristics and these are not fully restored by annealing at 500 °C. Oxidation via UV/O₃ treatments for *ex situ* carbon contamination removal and a variety of standard wet chemistries for oxide removal were also investigated. These O₃ and liquid cleans produced reduced the reverse current in the rectifiers, with no change in barrier height or ideality factor or degradation of reverse recovery characteristics.

II. EXPERIMENT

We used bulk β -phase, Sn-doped ($3.6 \times 10^{18} \text{ cm}^{-3}$) Ga₂O₃ single crystal wafers ($\sim 650 \mu\text{m}$ thick) with (001) surface orientation (Tamura Corporation, Japan) grown by the edge-defined film-fed growth method. Epitaxial layers (initially $\sim 15 \mu\text{m}$ thick) of lightly Si-doped n-type Ga₂O₃ ($\sim 2 \times 10^{16} \text{ cm}^{-3}$) were grown on these substrates by halide vapor phase epitaxy (HVPE) at Novel Crystal Technology. After growth, the episurface was planarized by chemical mechanical polishing to remove pits. The final epilayer thickness was $\sim 7 \mu\text{m}$. The x-ray diffraction full width at half maximum of the (402) peak was ~ 10 arc sec, and the dislocation density from etch pit observation was of the order of 10^3 cm^{-2} .

Diodes were fabricated by depositing full area back Ohmic contacts of Ti/Au (20 nm/80 nm) by E-beam evaporation. Ohmic behavior was achieved without the need for dry etching or ion implantation. The front sides were treated by different sequences of plasma, gas, or chemical processes prior to metallization. Solutions of HCl, NH₄OH, and HF are known to be effective for oxide removal. The surface exposure treatments we employed are shown in abbreviated form in Table I and consisted of the following seven different room temperature treatments: (i) O₃ exposure for 5–20 min in a UVOCS UV Ozone Cleaning System Model 70606B, (ii) rinsing in HCl (49%) for 2 or 4 min, (iii) rinsing in H₂O₂ (49%) for 2 or 4 min, (iv) rinsing in BOE for 2 or 4 min, (v) rinsing in HCl for 2 min followed by rinsing in H₂O₂ for 2 min or O₃ exposure for 2 min, (vi) exposure to an O₂ plasma for 1–8 min (power 50 W, gas flow rate 30 sccm, pressure 160 mTorr), or (vii) exposure to a CF₄ plasma for 1–8 min (power 50 W, gas flow rate 30 sccm, pressure 215 mTorr) (Technics, Micro-RIE). After these treatments, the front surfaces were deposited through a shadow mask with E-beam deposited Schottky contacts Ni/Au (20 nm/80 nm, area

$7.70 \times 10^{-4} \text{ cm}^2$) on the epitaxial layers. In some cases, the samples were annealed at 350–500 °C either before or after the Schottky contact deposition. This enables us to separate the effects of pure annealing and contact metal degradation. Figure 1 shows a schematic of the experimental sequence. Current–voltage (I–V) and capacitance–voltage (C–V) characteristics were recorded in air at room temperature on an Agilent 4145B parameter analyzer and 4284A Precision LCR Meter. We also measured the reverse recovery characteristics when switching from +1 to –5 V reverse bias.

III. RESULTS AND DISCUSSION

Examples of the rectifier I–V characteristics after different chemical treatments are shown in Fig. 2. In the case of liquid (HCl is shown as an example) rinses or O₃ cleaning, the forward current showed little change, and as summarized in Table I, the barrier height (Φ_B) and ideality factor (n) extracted from the forward I–V characteristics assuming thermionic emission was the dominant carrier transport mechanism, also showed little change from the reference sample values of $\Phi_B = 1.10$ and $n = 1.02$. These parameters were extracted from the linear range of the semilog plot of current density, J , vs V values for barrier height and ideality factor as $\Phi_B = (kT/e)[\ln(AA^{**}T^2/J_s)]$ and $n = (e/kT)[dV/d(\ln J)]$, where k is Boltzmann's constant, T is the temperature, e is the electronic charge, A is the diode area, and A^{**} is Richardson's constant.^{25,30–32}

By sharp contrast, plasma exposures to either O₂ or CF₄ discharges induced significant degradation of the rectification properties, as reflected in the reduced forward current and large increase in the reverse current. This was due to a reduction in barrier height and increase in ideality factor. For example, for O₂ plasmas, a 1 min exposure decreased Φ_B to 0.91 eV and n increased to 2.81. The latter value indicates the presence of significant generation-recombination in the carrier transport.²⁵ Continued exposure reduced Φ_B to 0.73 eV after 2 min, 0.64 eV after 4 min, and 0.60 eV after 8 min, with corresponding n values of 3.93 (2 min), 4.68 (4 min), and 4.84 (8 min). These ideality factors are unphysically large and indicate the presence of multiple current transport mechanisms beyond thermionic emission.^{2–4}

Similar large changes were observed for CF₄ plasmas, with Φ_B values of 0.79 eV after 1 or 2 min, 0.75 eV after 4 min, and 0.74 eV after 8 min, with corresponding n values in the range 3.4–4.1 (2–8 min). It is noteworthy that fluorine is readily incorporated into Ga₂O₃ during exposure to wet chemical solutions such as HF or by immersion in a fluorine-containing plasma.^{30,33} The fluorine atoms are strongly electronegative and become negatively charged, producing a compensation effect of Si donors by F-ions.³³ For chemical treatments such as rinsing in HF, there is an absence of plasma-induced surface damage and the fluorine incorporation leads to larger-than-expected effective barrier heights up to 1.46 eV for Pt (compared to 1.16–1.21 eV in reference samples).³³ Those results are consistent with F atoms acting as negative ions and compensating the ionized Si donors in the Ga₂O₃ to form neutral complexes, leading to additional

TABLE I. Summary of diode characteristics as a function of surface treatment prior to Schottky metal deposition.

Treatment	Schottky barrier height (eV)	Ideality factor	R_{ON} (m Ω cm ²)	J_R (μ A cm ⁻²) at 100 V V_R	n (cm ⁻³) from C–V	Rectification ratio (+1 V/–1 V)
Reference	1.10	1.02	4.23	14.08	$8.9\text{--}11 \times 10^{15}$	$\sim 10^9$
HCl, 2 min	1.04	1.03	7.66	13.33	1.19×10^{16}	$\sim 10^9$
HCl, 4 min	1.03	1.05	7.75	13.30	1.25×10^{16}	$\sim 10^9$
BOE, 4 min	1.07	1.06	6.66	14.94	—	—
O ₃ , 5 min	1.07	1.02	7.74	13.59	1.20×10^{16}	$\sim 10^9$
O ₃ , 20 min	1.08	1.02	9.44	12.6	1.26×10^{16}	$\sim 10^9$
H ₂ O ₂ , 2 min	1.00	1.06	6.97	13.8	—	$\sim 10^9$
H ₂ O ₂ , 4 min	1.02	1.05	6.48	13.6	—	$\sim 10^9$
HCl + H ₂ O ₂	1.01	1.06	8.86	13.2	—	$\sim 10^9$
HCl + O ₃	1.05	1.06	9.85	13.5	—	$\sim 10^9$
O ₂ plasma, 1 min	0.90	2.81	1.88	—	—	$\sim 10^3$
O ₂ plasma, 8 min	0.60	4.84	3.03	—	—	~ 20
O ₂ plasma, 8 min, anneal 450 °C	1.17	1.81	89.47	8.77	1.77×10^{16}	$\sim 10^3$
O ₂ plasma, 8 min, anneal 500 °C	1.17	1.76	76.43	—	1.93×10^{16}	$\sim 10^2$
CF ₄ plasma, 1 min	0.79	3.66	25.90	—	—	$\sim 10^2$
CF ₄ plasma, 8 min	0.74	4.10	49.10	—	—	~ 10
CF ₄ plasma, 8 min, anneal 450 °C	1.05	4.00	2.51×10^5	60.71	9.46×10^{15}	$\sim 10^0$
CF ₄ plasma, 8 min, anneal 500 °C	1.08	3.22	1.43×10^5	—	9.31×10^{15}	$\sim 10^0$
O ₂ plasma, 8 min, repattern	0.91	1.27	7.08	—	9.18×10^{15}	$\sim 10^4$
CF ₄ plasma, 8 min, repattern	0.84	1.68	8.63×10^2	—	7.81×10^{15}	$\sim 10^5$

surface depletion.³⁰ In the case when plasma damage is present, barrier lowering occurs, as evidenced by the increased forward and reverse leakage in diodes fabricated on those surfaces.^{26,27} Annealing at a gate electrode-

compatible temperature of 400 °C can partially remove the plasma-induced damage. This is also consistent with the temperatures at which point defect damage in Ga₂O₃ is observed to anneal out.²⁹

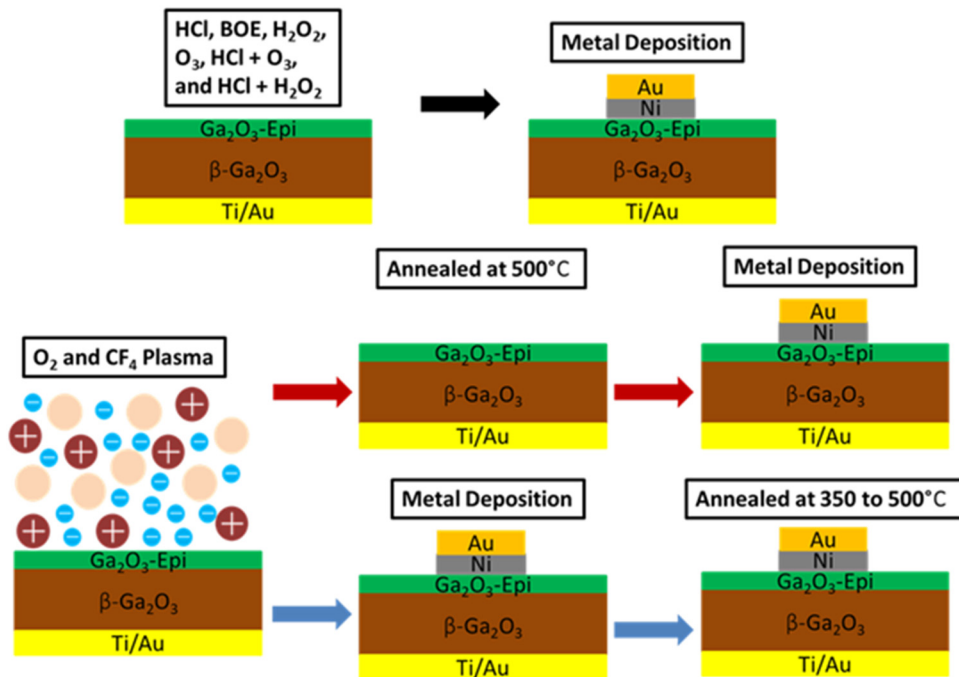
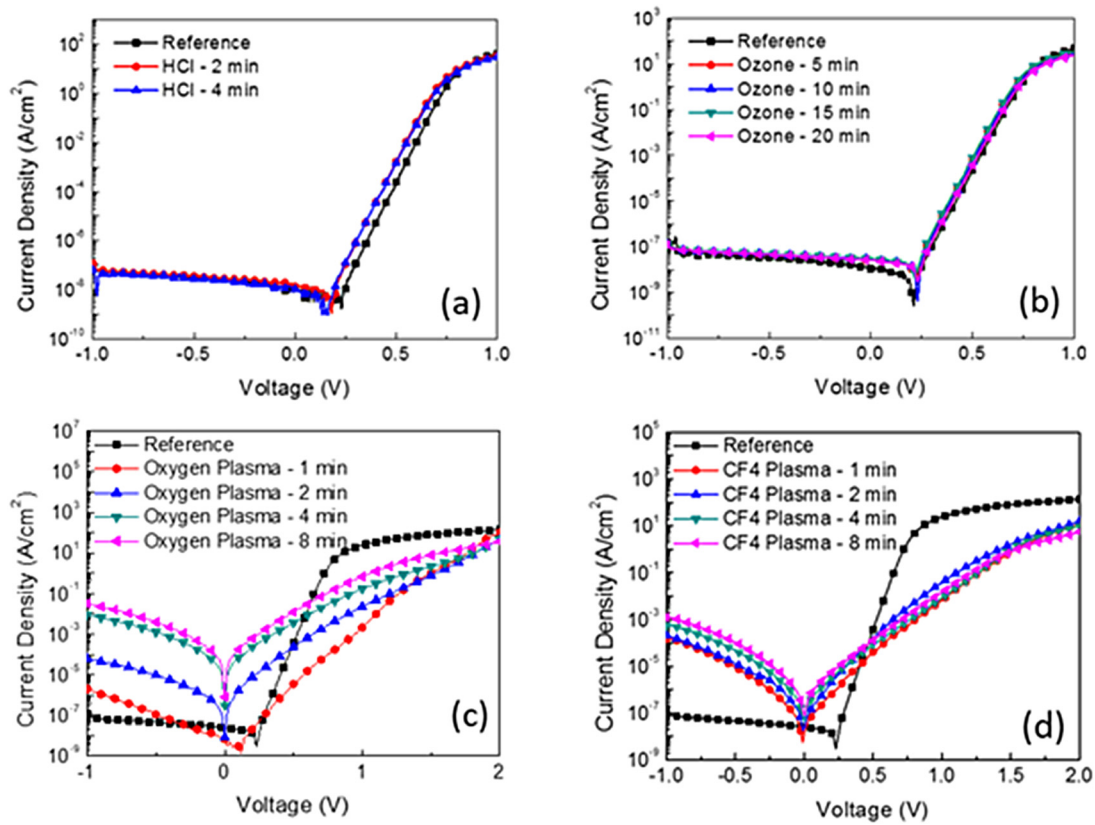
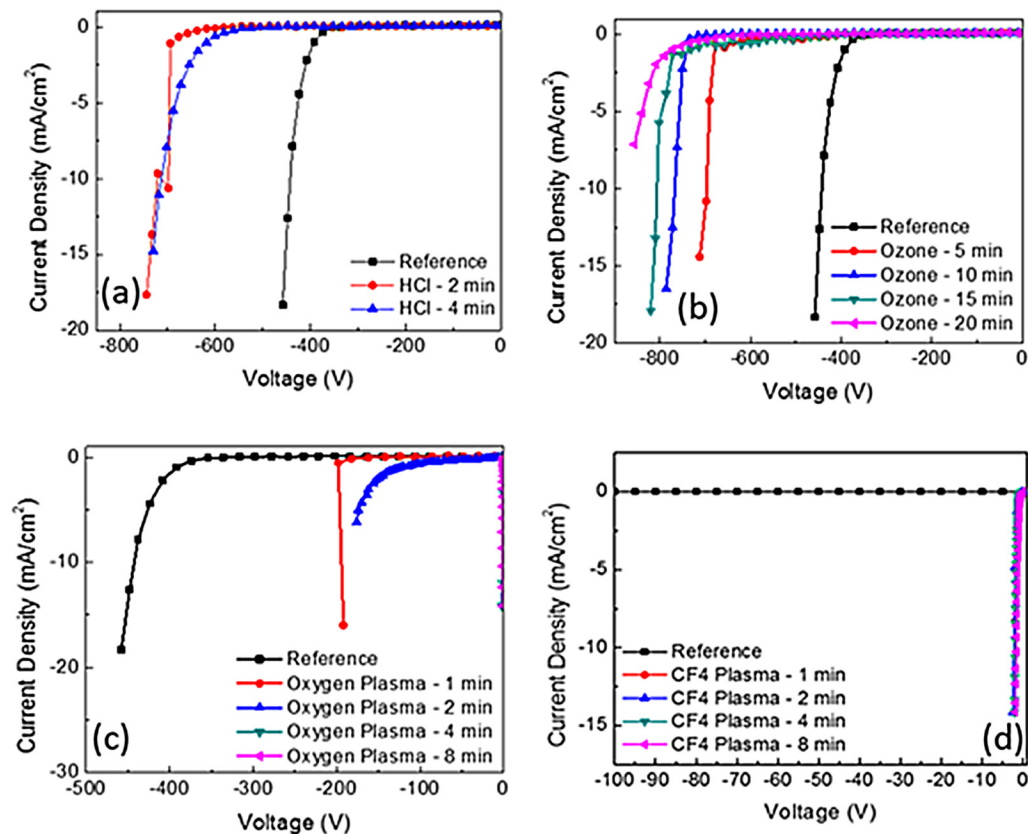


FIG. 1. Schematic of process sequence. The samples were exposed to liquid or gas chemical mixtures or plasmas, followed by either metal deposition and annealing with these in place, or annealing then metal deposition.

FIG. 2. Forward I–V characteristics from samples exposed to (a) HCl, (b) O₃, (c) O₂ plasma, or (d) CF₄ plasma.FIG. 3. Reverse I–V characteristics from samples exposed to (a) HCl, (b) O₃, (c) O₂ plasma, or (d) CF₄ plasma.

The increase of the ideality factors and the lowering of Φ_B are common phenomena in damaged semiconductor surfaces and usually attributed to thin interfacial layers between the metal and the semiconductor, or the creation of near-surface point or extended defects.²⁵ These induce current transport mechanisms in addition to thermionic emission, namely, tunneling and thermionic-field emission. The effect of thermionic-field emission can be calculated as a temperature independent effective tunneling barrier lowering, but in our case, this is of the order of 0.03 eV, for $V=0.6$, much lower than observed.

Figure 3 shows representative reverse I–V characteristics after several of the surface treatments in more detail. The ozone or liquid treatments lead to improved reverse breakdown voltage. This can be a result of the removal of surface contamination such as adventitious carbon (which ozone is known to remove) or native oxides which promote leakage current. By contrast, both of the plasma treatments degrade the reverse breakdown by reducing the barrier height. The effect of the nonplasma chemical treatments on reverse current density is summarized in Fig. 4. The BOE treatment was the only one of these to degrade the current, while HCl, H₂O₂, combinations of these two, or O₃ all produced reduced reverse current. It was reported that HCl solutions produced the lowest coverages of oxygen on AlN and GaN surfaces, respectively, with residual F and Cl tying up dangling bonds at the nitride surfaces hindering reoxidation^{34,35} and a similar mechanism may be present for Ga₂O₃. Surface cleaning must be efficient in the removal of native oxides, organic contaminants, metallic impurities, particulate contaminants, adsorbed molecules, and residual species.^{34–36}

The effect of annealing is relevant since the device processing sequence can usually be varied to include an annealing step prior to Schottky metal deposition, as we show in Fig. 1, provided the Ohmic contact that is already in place can withstand the temperature cycle. Figure 5 shows examples of reverse I–V characteristics from samples exposed to CF₄ plasmas for different durations and then annealed at 350 °C (top) or 450 °C (bottom) prior to annealing. The characteristics are not recovered by 350 °C anneals, but 450 °C brings significant recovery and even an increase in breakdown due to the fluorine compensation effect. In the case of

pure surface damage with O₂ plasmas, the reverse breakdown did not generally improve over the control value after 350 or 450 °C anneals, except in the case of the samples exposed for 8 min prior to annealing, where the plasma damage led to deep trap formation and slightly higher breakdown in the range 480–620 V.

Figure 6 summarizes the effect of annealing on the metallized reference and plasma treated samples. The reverse breakdown is degraded by annealing due to contact reaction with the Ga₂O₃, even at 350 °C. This is evident from the fact that when we repattern these annealed rectifiers and place fresh Schottky contacts on the annealed surface, the reverse breakdown voltage is virtually restored. The plasma treated samples show a much reduced breakdown after exposure to either O₂ or CF₄. In the latter case, the F compensation effect is most pronounced after 450 °C annealing, whereas higher temperatures remove this and restore the original breakdown voltage. Deposition of fresh contacts on the annealed surface produces the same breakdown value as on the unannealed reference.

Room temperature C–V measurements were also performed to extract dopant concentration (N_D) according to $1/C^2 = (2/e\epsilon_s N_D)[e\Phi_B - V - (E_C - E_F) - (kT/e)]$, where ϵ_s is

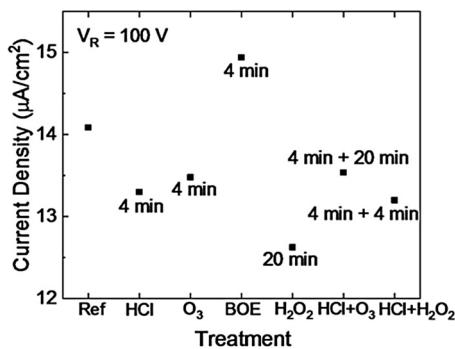


FIG. 4. Reverse leakage at a bias of -100 V for different surface treatments prior to metallization.

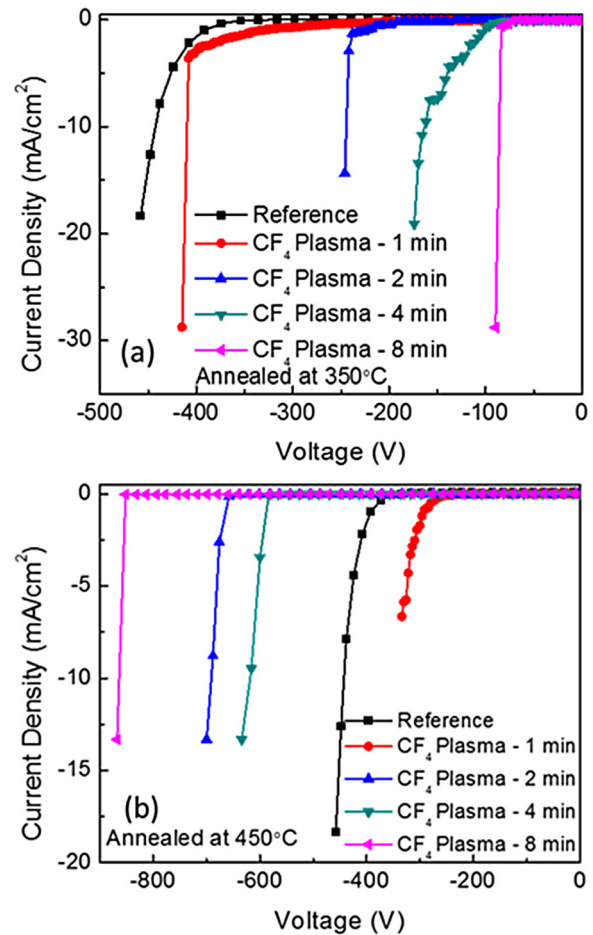


FIG. 5. Reverse I–V characteristics from samples before and after exposure to CF₄ plasmas for different times, followed by annealing at either (a) 350 °C or (b) 450 °C with the metallization in place.

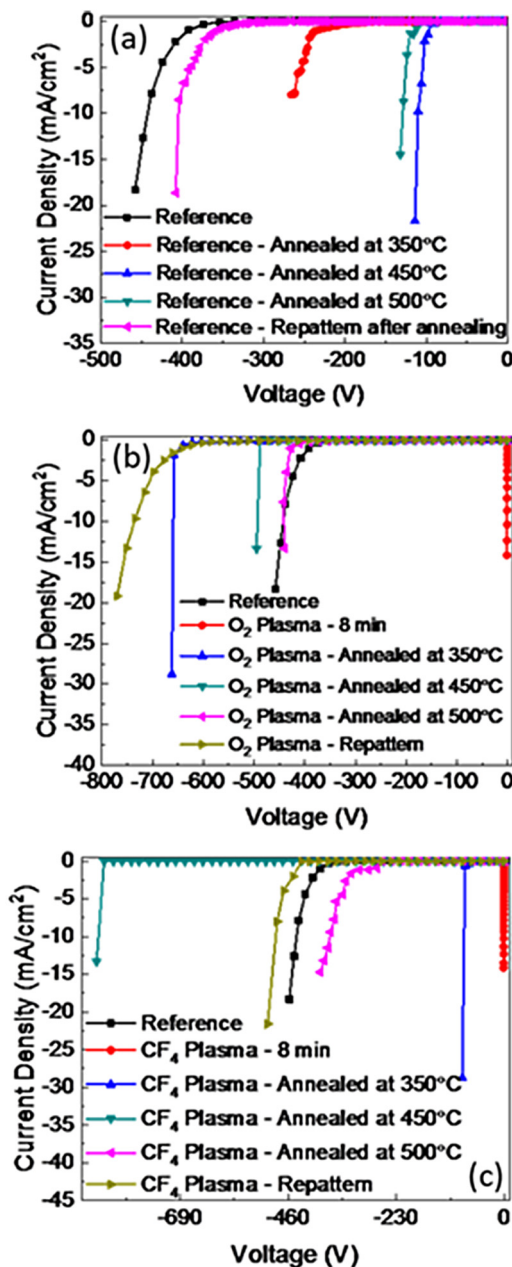


FIG. 6. Reverse I–V characteristics from (a) reference samples annealed at different temperatures, (b) before and after exposure to O₂ plasmas for 8 min, followed by annealing at 350–500 °C, (c) before and after exposure to CF₄ plasmas for 8 min, followed by annealing at 350–500 °C. The metallization was in place during annealing and fresh contacts were deposited on the annealed surfaces after the 500 °C anneal.

the permittivity, E_C is the conduction band minima, and E_F is the Fermi level. Figure 7 shows these plots for the plasma exposed samples before and after annealing. The doping densities extracted from these plots show values of 8.9×10^{15} – $1.1 \times 10^{16} \text{ cm}^{-3}$ for the reference samples, which were only cleaned with acetone and isopropyl alcohol organic solvent. For the wet chemical and O₃ treated samples, the carrier concentration is in a range of 1.19 – $1.26 \times 10^{16} \text{ cm}^{-3}$. Since the C–V measurements are quite surface sensitive, the carrier concentration extrapolated from the true reference sample might not be a good representation of the doping density for

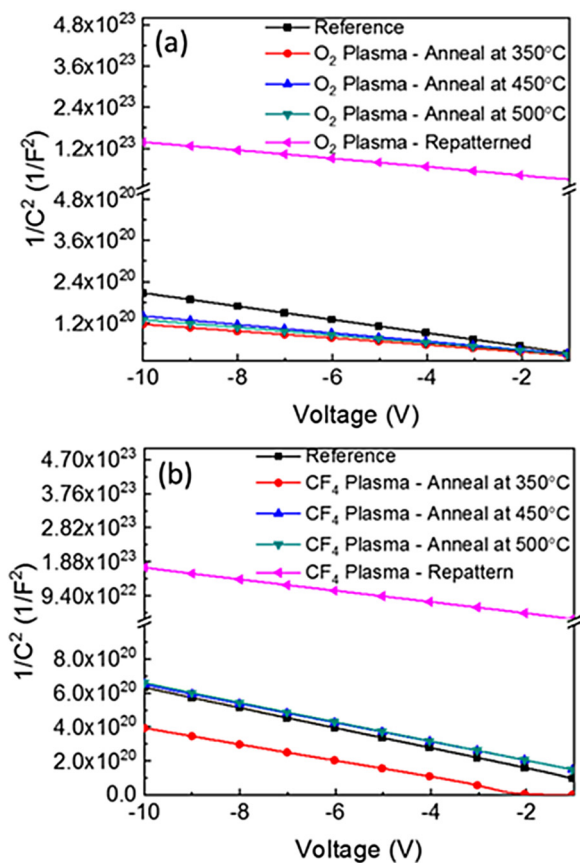


FIG. 7. C⁻²–V plots for samples exposed to O₂ or CF₄ plasmas for 1–8 min, followed by annealing at 350–500 °C with the metallization in place and metallization after the 500 °C annealing process.

the drift region, which could explain a wide span of the carrier concentration for the reference samples. Furthermore, with the consistency of the carrier concentrations calculated from both wet chemical and O₃ treated samples, they are considered as the baseline for the drift region doping concentration. In comparison with the baseline doping concentration, the drift region carrier concentration shows a slight increase for O₂ plasma exposed samples annealed at 350–500 °C with a range of 1.77 – $1.93 \times 10^{16} \text{ cm}^{-3}$, which could be caused by the ion bombardment damage on the sample surface during the plasma exposure and the metal diffusion process during the annealing steps. CF₄ plasma exposed samples that annealed at 350–500 °C show a decreasing trend of the carrier concentration in a range of 1.21×10^{16} to $9.31 \times 10^{15} \text{ cm}^{-3}$, and this is consistent with what was previously reported.³⁰ The C–V measurements for both O₂ and CF₄ plasma exposed samples with fresh Schottky contact after 500 °C annealing reveal a decrease in carrier concentration for the epilayer in comparison to the baseline and the carrier concentration is 9.18 and $7.81 \times 10^{15} \text{ cm}^{-3}$, respectively. This would explain the increasing of diode breakdown voltage for both O₂ and CF₄ plasma exposed samples after 500 °C annealing. Note that these are averages over a depth of $\sim 3 \mu\text{m}$ and the value could be different at the immediate surface, as reflected in the reduced barrier heights.

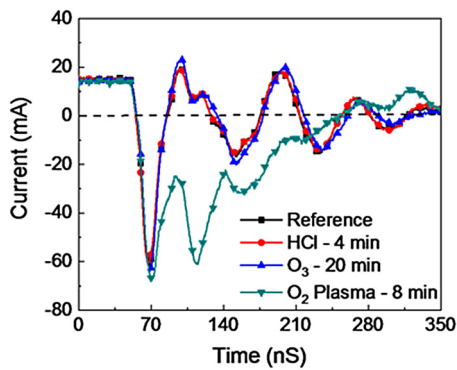


Fig. 8. Reverse recovery characteristics for diodes fabricated with different surface treatments. All the samples were switched from +2 to -10 V.

Figure 8 shows the reverse recovery characteristics when switching from +2 to -10 V, with a recovery time of 33.5 ns. The HCl and ozone treated samples did not show any deviation of reverse recovery from the reference sample. The double peaks for the plasma treated sample are a result of the device not completely turning off due to the high leakage current.

What are the main defects expected in the near-surface region of Ga₂O₃? Epitaxial films of β -Ga₂O₃ grown by HVPE on native substrates have electron traps near Ec-0.6 eV, Ec-0.75 eV, and Ec-1.05 eV, similar to the E1, E2, and E3 electron traps observed in bulk β -Ga₂O₃ crystals.^{37–42} Proton irradiation increases the density of E2 (Ec-0.75 eV) and Ec-2.3 eV traps, suggesting these incorporate native defects.³⁷ The concentration of these traps in the HVPE films is 1–2 orders of magnitude lower than in bulk material.³⁷ There are three hole traps in the lower half of the bandgap, namely, H1, H2, and H3, with activation energies 0.2, 0.4, and 1.3 eV, respectively. The H1 peak is suggested to correspond to the transition of polaronic states of self-trapped holes to mobile holes in the valence band. The H2 feature is assigned to overcoming of the electron capture barrier of centers responsible for persistent photocapacitance at $T < 250$ K. The H3 peak is produced by detrapping of holes from Ev + 1.3 eV hole traps related to Ga⁺ acceptors. Deák *et al.*⁴³ suggested from a theoretical study that all photoluminescence bands of beta-Ga₂O₃ can be explained by electron recombination at trapped holes, with different intrinsic defects or nitrogen acting as hole traps. With the exception of gallium interstitials, which can act as shallow donors, all other intrinsic defects are deep. Ga vacancies are the main compensating acceptors in n-type samples, while both oxygen interstitials and vacancies act as hole traps, in addition to small hole polarons.^{44–48} Electron paramagnetic resonance (EPR) studies in both n-type and semi-insulating Ga₂O₃ after irradiation found one dominant induced paramagnetic defect with the characteristics of a V_{Ga} center.^{46–48} Korhonen *et al.*⁴⁶ investigated the electrical compensation in n-type Ga₂O₃ by V_{Ga} using positron annihilation spectroscopy and estimated a V_{Ga} concentration of $\geq 5 \times 10^{18} \text{ cm}^{-3}$ in undoped and Si-doped samples. Since theoretical calculations predict that these V_{Ga} should be in a negative charge state for n-type samples,³⁴ they will compensate the n-type doping.⁴⁸ Kananen *et al.*^{47,48} used EPR to demonstrate the

presence of both doubly ionized (V_{Ga}^{2-}) and singly ionized (V_{Ga}^-) acceptors at room temperature in CZ Ga₂O₃. They observed singly ionized gallium vacancies V_{Ga}^- in neutron irradiated β -Ga₂O₃. Oxygen vacancy formation is found to depend on the position of the Fermi level and is unlikely to be shallow donors.^{45,49} During high temperature thermal processing, it is likely that oxygen is lost from the surface through the reaction $\text{Ga}_2\text{O}_3 \rightarrow 2\text{GaO} + 0.5\text{O}_2(\text{g})$, but the oxygen vacancies will not have the same effect on conductivity as the dominant Ga vacancies. Chemical or ion-free processes such as UV/O₃ do not have sufficient energy to disrupt the Ga₂O₃ surface but energetic plasmas induce native point defects that alter the near-surface electrical properties.

IV. SUMMARY AND CONCLUSIONS

The Ga₂O₃ surface is shown to be particularly sensitive to plasma-induced damage, leading to the introduction of generation-recombination centers that degrade the Schottky characteristics. These are most likely related to Ga vacancies. This damage is partially recovered by 500 °C annealing. Standard chemical cleans involving UV/O₃ or acid rinses do not degrade the near-surface electrical properties.

ACKNOWLEDGMENTS

The project at UF was sponsored by the Department of the Defense, Defense Threat Reduction Agency, No. HDTRA1-17-1-011, monitored by Jacob Calkins. The content of the information does not necessarily reflect the position or the policy of the federal government, and no official endorsement should be inferred. Research at NRL was supported by the Office of Naval Research, partially under Award No. N00014-15-1-2392.

- ¹A. Kuramata, K. Koshi, S. Watanabe, Y. Yamaoka, T. Masui, and S. Yamakoshi, *Jpn. J. Appl. Phys. Part 1* **55**, 1202A2 (2016).
- ²H. Von Wenckstern, *Adv. Electron. Mater.* **3**, 1600350 (2017).
- ³M. Higashiwaki, K. Sasaki, H. Murakami, Y. Kumagai, A. Koukitu, A. Kuramata, T. Masui, and S. Yamakoshi, *Semicond. Sci. Technol.* **31**, 034001 (2016).
- ⁴S. J. Pearton, Jiancheng Yang, Patrick H. Cary IV, F. Ren, Jihyun Kim, Marko J. Tadjer, and Michael A. Mastro, *Appl. Phys. Rev.* **5**, 011301 (2018).
- ⁵Z. Galazka *et al.*, *ECS J. Solid State Sci. Technol.* **6**, Q3007 (2017).
- ⁶M. J. Tadjer *et al.*, *J. Electron. Mater.* **45**, 2031 (2016).
- ⁷S. Rafique, L. Han, A. T. Neal, S. Mou, M. J. Tadjer, R. H. French, and H. Zhao, *Appl. Phys. Lett.* **109**, 132103 (2016).
- ⁸M. Baldini, M. Albrecht, A. Fiedler, K. Irmscher, R. Schewski, and G. Wagner, *ECS J. Solid State Sci. Technol.* **6**, Q3040 (2017).
- ⁹Serdar Okur, Gary S. Tompa, Nick Sbrokeck, Tom Salagaj, Volker Blank, Bernd Henninger, Michele Baldini, Günter Wagner, Zbigniew Galazka, Yao Yao, J. Rokholt, Robert F. Davis, Lisa M. Porter, and Abraham Belkind, *Vacuum Technology and Coating* (2017), pp. 31–39.
- ¹⁰M. A. Mastro, A. Kuramata, J. Calkins, J. Kim, F. Ren, and S. J. Pearton, *ECS J. Solid State Sci. Technol.* **6**, P356 (2017).
- ¹¹B. Bayraktaroglu, Assessment of Gallium Oxide Technology, Air Force Research Lab, Devices for Sensing Branch, Aerospace Components & Subsystems Division, Report AFRL-RY-WP-TR-2017-0167, 2017, see <http://www.dtic.mil/dtic/tr/fulltext/u2/1038137.pdf>
- ¹²Masataka Higashiwaki and Gregg H. Jessen, *Appl. Phys. Lett.* **112**, 060401 (2018).
- ¹³A. Merkert, T. Krone, and A. Mertens, *IEEE Trans. Power Electron.* **29**, 2245 (2014).

- ¹⁴Jin Wang, Victor Veliadis, Jon Zhang, Yazan Alsmadi, Peter R. Wilson, and Mark J. Scott, *IEEE Power Electron. Mag.* **5**, 40 (2018).
- ¹⁵A. Q. Huang, *Proc. IEEE* **105**, 2019 (2017).
- ¹⁶X. She, A. Q. Huang, O. Lucia, and B. Ozpineci, *IEEE Trans. Ind. Electron.* **64**, 8193 (2017).
- ¹⁷T. J. Flack, B. N. Pushpakaran, and S. B. Bayne, *J. Electron. Mater.* **45**, 2673 (2016).
- ¹⁸K. J. Chen, O. Häberlen, A. Lidow, Chun Lin Tsai, T. Ueda, Y. Uemoto, and Y. Wu, *IEEE Trans. Electron Devices* **64**, 779 (2017).
- ¹⁹Yao Yao, Raveena Gangireddy, Jaewoo Kim, Kalyan Kumar Das, Robert F. Davis, and Lisa M. Porter, *J. Vac. Sci. Technol. B* **35**, 03D113 (2017).
- ²⁰R. Suzuki, S. Nakagomi, Y. Kokubun, N. Arai, and S. Ohira, *Appl. Phys. Lett.* **94**, 222102 (2009).
- ²¹K. Sasaki, M. Higashiwaki, A. Kuramata, T. Masui, and S. Yamakoshi, *IEEE Electron Device Lett.* **34**, 493 (2013).
- ²²Hideori Ishikawa, Setsuko Kobayashi, and Y. Koide, *J. Appl. Phys.* **81**, 1315 (1997).
- ²³Houqiang Fu, Hong Chen, Xuanqi Huang, Izak Baranowski, Jossue Montes, Tsung-Han Yang, and Yuji Zhao, *IEEE Trans. Electron Devices* **65**, 3507 (2018).
- ²⁴J. Bae, H. W. Kim, I. H. Kang, G. Yang, and J. Kim, *Appl. Phys. Lett.* **112**, 122102 (2018).
- ²⁵A. Jayawardena, A. C. Ahyi, and S. Dhar, *Semicond. Sci. Technol.* **31**, 115002 (2016).
- ²⁶Jiancheng Yang, S. Ahn, Fan Ren, S. J. Pearton, Rohit Khanna, Kristen Bevin, Dwarakanath Geerpuram, and Akito Kuramata, *J. Vac. Sci. Technol. B* **35**, 031205 (2017).
- ²⁷Jiancheng Yang *et al.*, *J. Vac. Sci. Technol. B* **35**, 051201 (2017).
- ²⁸G. Yang, S. Jang, F. Ren, S. J. Pearton, and J. Kim, *ACS Appl. Mater. Interfaces* **9**, 40471 (2017).
- ²⁹J. Yang *et al.*, *J. Vac. Sci. Technol. B* **36**, 011206 (2018).
- ³⁰Jiangcheng Yang, Chaker Fares, F. Ren, Ribhu Sharma, Erin Patrick, Mark E. Law, S. J. Pearton, and Akito Kuramata, *J. Appl. Phys.* **123**, 165706 (2018).
- ³¹S. K. Cheung and N. W. Cheung, *Appl. Phys. Lett.* **49**, 85 (1986).
- ³²Ang Li, Qian Feng, Jincheng Zhang, Zhuang Hu, Zhaoqing Feng, Ke Zhang, Chunfu Zhang, Hong Zhou, and Yue Hao, *Superlattices Microstruct.* **119**, 212 (2018).
- ³³Keita Konishi, Ken Goto, Hisashi Murakami, Yoshinao Kumagai, Akito Kuramata, Shigenobu Yamakoshi, and Masataka Higashiwaki, *Appl. Phys. Lett.* **110**, 103506 (2017).
- ³⁴S. W. King, J. P. Barnak, M. D. Bremser, K. M. Tracy, C. Ronning, R. F. Davis, and R. J. Nemanich, *J. Appl. Phys.* **84**, 5248 (1998).
- ³⁵L. L. Smith, S. W. King, R. J. Nemanich, and R. F. Davis, *J. Electron. Mater.* **25**, 805 (1996).
- ³⁶W. J. Mccouch, B. P. Wagner, Z. J. Reitmeier, R. F. Davis, C. Pandarinath, B. J. Rodriguez, and R. J. Nemanich, *J. Vac. Sci. Technol. A* **23**, 72 (2005).
- ³⁷A. Y. Polyakov *et al.*, *Appl. Phys. Lett.* **112**, 032107 (2018).
- ³⁸Z. Zhang, E. Farzana, A. R. Arehart, and S. A. Ringel, *Appl. Phys. Lett.* **108**, 052105 (2016).
- ³⁹Yoshitaka Nakano, *ECS J. Solid State Sci. Technol.* **6**, P615 (2017).
- ⁴⁰M. E. Ingebrigtsen, J. B. Varley, A. Yu. Kuznetsov, B. G. Svensson, G. Alfieri, A. Mihaila, U. Badstübner, and L. Vines, *Appl. Phys. Lett.* **112**, 042104 (2018).
- ⁴¹K. Irmscher, Z. Galazka, M. Pietsch, R. Uecker, and R. Fornari, *J. Appl. Phys.* **110**, 063720 (2011).
- ⁴²Esmat Farzana, Elaheh Ahmadi, James S. Speck, Aaron R. Arehart, and Steven A. Ringel, *J. Appl. Phys.* **123**, 161410 (2018).
- ⁴³Peter Deák, Quoc Duy Ho, Florian Seemann, Bálint Aradi, Michael Lorke, and Thomas Frauenheim, *Phys. Rev. B* **95**, 075208 (2017).
- ⁴⁴E. Chikoidze *et al.*, *Mater. Today Phys.* **3**, 118 (2017).
- ⁴⁵J. B. Varley, J. R. Weber, A. Janotti, and C. G. Van de Walle, *Appl. Phys. Lett.* **97**, 142106 (2010).
- ⁴⁶E. Korhonen, F. Tuomisto, D. Gogova, G. Wagner, M. Baldini, Z. Galazka, R. Schewski, and M. Albrecht, *Appl. Phys. Lett.* **106**, 242103 (2015).
- ⁴⁷B. E. Kananen, L. E. Halliburton, K. T. Stevens, G. K. Foundos, K. B. Chang, and N. C. Giles, *Appl. Phys. Lett.* **110**, 202104 (2017).
- ⁴⁸B. E. Kananen, N. C. Giles, L. E. Halliburton, G. K. Foundos, K. B. Chang, and K. T. Stevens, *J. Appl. Phys.* **122**, 215703 (2017).
- ⁴⁹L. Dong, R. Jia, B. Xin, B. Peng, and Y. Zhang, *Sci. Rep.* **7**, 40160 (2017).